International Journal of Mass Spectrometry 446 (2019) 116231

Contents lists available at ScienceDirect

International Journal of Mass Spectrometry

journal homepage: www.elsevier.com/locate/ijms

Measurement of the asymmetric UO_2^{2+} stretching frequency for $[U^{VI}O_2(F)_3]^-$ using IRMPD spectroscopy

Irena Tatosian [a], Luke Metzler [a], Connor Graca [a], Amanda Bubas [a, 1], Theodore Corcovilos [b, **], Jonathan Martens [c], Giel Berden [c], Jos Oomens [c, d], Michael J. Van Stipdonk [a, *]

[a] Department of Chemistry and Biochemistry, Duquesne University, 600 Forbes Ave, Pittsburgh, PA, 15262, USA
[b] Department of Physics, Duquesne University, 600 Forbes Ave, Pittsburgh, PA, 15262, USA
[c] Radboud University Nijmegen, Institute for Molecules and Materials, FELIX Facility, Toernooiveld 7, 6525ED, Nijmegen, the Netherlands
[d] van 't Hoff Institute for Molecular Sciences, University of Amsterdam, Science Park 904, 1098XH, Amsterdam, the Netherlands

ARTICLE INFO

Article history:
Received 23 July 2019
Received in revised form
10 September 2019
Accepted 16 September 2019
Available online 17 September 2019

Keywords:
Electrospray ionization
Infrared multiple photon photodissociation
Uranyl ion
Asymmetric stretching frequency
Tandem mass spectrometry

ABSTRACT

In a previous study [*Int. J. Mass Spectrom.* **2010**; *297*: 67–75], the asymmetric O=U=O stretch (ν_3) was measured for anionic uranyl complexes with composition $[UO_2(X)_3]^-$, X = Cl^-, Br^- and I^-. Within this group of complexes, the ν_3 frequency red-shifts following the trend I > Br > Cl, suggesting concomitant weakening of the U=O bonds. However, a value for $[UO_2(F)_3]^-$ was not measured, which prevented a comprehensive comparison of measured ν_3 positions to computed frequencies from density functional theory (DFT) calculations. Because the shift in ν_3 is predicted to be most dramatic when X = F, we revisited these species using infrared multiple-photon photodissociation spectroscopy. As in our earlier study, a modest red-shift to the ν_3 vibration of ~ 6 cm^{-1} was observed for X = I^-, Br-, and Cl^-, and the position of the frequency follows the trend $I^- > Br^- > Cl^-$. The value measured for $[UO_2(F)_3]^-$ is ~43 cm^{-1} lower than the one measured for $[UO_2(Cl)_3]^-$. Overall, the trend with respect to ν_3 position is reproduced well by computed frequencies from DFT.

1. Introduction

Developing a comprehensive understanding of the structure and bonding of uranium complexes [1] remains important to (a) the development of nuclear fuel processing methods [2]; (b) studies of the migration and fate of the element in the environment [3,4] and (c) elucidation of 5-f element chemistry in general. Electrospray ionization (ESI) is an effective tool for production of gas-phase complexes containing uranium in high oxidation states [5]. Our group was among the first to use ESI to generate gas-phase complexes containing the uranyl ion ($U^{VI}O_2^{2+}$) for studies of intrinsic structure and reactivity (i.e. outside of the influence of solvent or other condensed phase effects) in a species-specific fashion [6–26].

One focus of our research effort in this area has been on the use of wavelength-selective infrared multiple photon photodissociation (IRMPD) spectroscopy to determine ion (geometric) structure, and probe the extent to which ligand-specific binding influences the position of the asymmetric O=U=O stretch (ν_3) [12–16,18,27,28] (it is known that the uranium-oxygen bonds in the uranyl dication, UO_2^{2+}, are weakened by electron donation to the uranium metal center by coordinating nucleophiles [29–37]). In a previous study [12], the gas-phase infrared spectra of discrete UO_2^{2+} complexes coordinated by acetone (aco) and/or acetonitrile (acn) were used to evaluate systematic trends of ligation on the position of ν_3, and for comparison with frequencies predicted by density functional theory (DFT). The ν_3 value of 1017 cm^{-1} was measured for $[UO_2(aco)_2]^{2+}$, and the frequency systematically red shifted to 1000 and 988 cm^{-1} with addition of a third and fourth acetone ligand, respectively (consistent with increased donation of electron density to the U center with higher coordination number). Similar trends were observed for $[UO_2(acn)_n]^{2+}$ complexes, although the ν_3 frequencies were greater than those measured for acetone complexes having the same coordination number. This observation was

* Corresponding author.
** Corresponding author.
E-mail addresses: corcovilost@duq.edu (T. Corcovilos), vanstipdonkm@duq.edu (M.J. Van Stipdonk).
[1] Current address: Department of Chemistry, University of Utah, 215 1400 E, Salt Lake City, UT 84112.

https://doi.org/10.1016/j.ijms.2019.116231
1387-3806/

consistent with the fact that acn is a weaker nucleophile than aco.

In another earlier investigation [38], the IRMPD spectra of a series of positively-charged complexes with composition $[UO_2(X)(aco)_3]^+$ (where X = F, Cl, Br or I), generated by ESI, were collected using a Fourier-transform ion cyclotron resonance (FT-ICR) mass spectrometer and IR radiation from the FELIX free-electron laser. For these cationic species, the measurements showed that the ν_3 frequency was insensitive to the particular halide when X was Cl^-, Br^- or I^-. The ν_3 peak in the spectrum of $[UO_2(F)(aco)_3]^+$ was 9 cm^{-1} lower, indicating stronger coordination and increased donation of charge to the metal center in this complex.

In the same set of experiments, the IRMPD spectra of the negatively charged complexes $[UO_2(X)_3]^-$ (where X = Cl^-, Br^- and I^-) were collected. Within this group, the ν_3 frequency shifted to lower values, following the trend I > Br > Cl; however, no (experimental) photodissociation signal was observed for the $[UO_2(F)_3]^-$ complex, which prevented a comprehensive comparison of measured ν_3 positions to computed frequencies from DFT calculations. Because the shift in ν_3 is predicted to be most dramatic when X = F, we revisited these species using wavelength-selective infrared photodissociation in a quadrupole ion trap mass spectrometer. The specific goals here were: (a) to measure ν_3 for $[UO_2(F)_3]^-$, (b) to compare ν_3 for $[UO_2(F)_3]^-$ to values for $[UO_2(Cl)_3]^-$, $[UO_2(Br)_3]^-$ and $[UO_2(I)_3]^-$ measured under similar experimental conditions and (c) establish the extent to which the *trend* in experimentally-measured shift to ν_3 is captured by DFT calculations.

2. Experimental methods

2.1. Sample preparation

The samples used to prepare gas-phase $[UO_2(X)_3]^-$ were created by digestion of 2–3 mg $U^{VI}O_3$ (Strem Chemicals, Newburyport, MA), corresponding to approximately 7 x 10^{-6} to 1 x 10^{-5} mol, using a 2-fold mole excess of the respective acids (HF, HCl, HBr and HI, Sigma Aldrich, St. Louis, MO) and 200 μL of deionized/distilled H_2O in a glass scintillation vial. To assist digestion, the solutions were gently heated on a hot plate at 70 °C for several hours. Caution: uranium oxide is radioactive (α- and γ-emitter), and proper shielding, waste disposal, and personal protective gear should be used when handling the material. When cooled, 20 μL of the resulting solution were diluted with 300 μL of 50:50 (by volume) H_2O/CH_3OH and used without further work up as the spray solution for ESI-MS.

2.2. IRMPD spectroscopy

IRMPD experiments were performed at the Free Electron Laser for Infrared eXperiments (FELIX) laboratory [39]. The respective $[UO_2(X)_3]^-$ precursor ions were generated by ESI using the prepared solutions. IRMPD spectra were acquired using a quadrupole ion trap mass spectrometer (Bruker) which has been modified [40] such that the high-intensity tunable IR beam from FELIX can be directed into the ion packet, resulting in multiphoton dissociation that is appreciable only when the IR frequency is in resonance with an adequately high absorption vibrational mode of the particular mass-selected complex being studied. The FEL produces ~5 μs long IR pulses with an energy of typically 40 mJ, which are in the form of a sequence of ~1 ps long micropulse at a 1 GHz repetition rate. The wavelength of the radiation was tuned between 10 and 12 μm in these experiments.

2.3. Density functional theory calculations

Geometry optimizations for potential product ion structures were performed using the B3LYP [41–43], PBE0 [44,45], M06-L [46] and SVWN [47] functionals, the MWB60 pseudopotential and associated basis set on U, MWB46 pseudopotential and associated basis set on I, and the triple-zeta 6-311 + G(d), aug-cc-pvtz or 6-311 + G(3df) basis sets on all other atoms. The pseudopotential and functionals were chosen because they have been used in previous studies of gas-phase U species, including measurements of the O═U═O stretching frequencies. The basis sets used here have also been employed in previous studies. Our intent was not to rigorously assess the accuracy of the DFT method for determining U═O or U-X bond lengths, or evaluation of DFT methods for prediction of absolute stretching frequencies, but instead to ensure that *consistent trends are identified with respect to the influence of the halide ligands on the shift to the ν_3 frequency*. We note that extensive calculations to support studies of bonding in uranyl-halide species have been carried out by Vallet and coworkers [48] and Wang, Li and coworkers [49], and for more general uranyl species by other [50,51], to which we refer the reader for discussions of accuracy of the computational approaches.

In all cases, geometry optimizations were performed with an ultrafine integration grid and a tight convergence criterion. Vibrational frequency calculations were performed, using the respective optimized geometries, to ensure that all species were true minima (i.e. no imaginary frequencies) and for comparison to experimental IRMPD spectra. The Gaussian 09 software package [52] was used for all calculations.

3. Results and discussion

3.1. IRMPD measurements

In our earlier investigation [34], abundant $[UO_2(X)_3]^-$ complexes were generated by ESI using each of the four uranyl-halide materials. Different photofragmentation behavior was noted for the respective precursors: no photodissociation products were observed for $[UO_2(F)_3]^-$; $[UO_2(Cl)_3]^-$ dissociated solely by loss of (neutral) $[UO_2(Cl)_2]$ to form Cl^- (shown in general as reaction **1**); $[UO_2(I)_3]^-$ eliminated iodine radical to create $[UO_2(I)_2]^-$ (shown in general as reaction **2**) and the $[UO_2(Br)_3]^-$ precursor fragmented by both pathways. The trends in dissociation behavior were in good general agreement with computed reaction energetics [34].

$$[U^{VI}O_2(X)_3]^- \rightarrow [U^{VI}O_2(X)_2]^- + X^\cdot \quad (1)$$

$$[U^{VI}O_2(X)_3]^- \rightarrow [U^{V}O_2(X)_2]^- + X^\cdot \quad (2)$$

Using IRMPD in the FT-ICR instrument, the uranyl ν_3 frequencies measured for the three complexes that exhibited dissociation channels ranged from 935 cm^{-1} for $[UO_2(Cl)_3]^-$ to 941 cm^{-1} for $[UO_2(Br)_3]^-$ to 948 cm^{-1} for $[UO_2(I)_3]^-$.

In the present study, all four anionic complexes were also generated using ESI and the quadrupole ion trap analyzer. For $[UO_2(Cl)_3]^-$, $[UO_2(Br)_3]^-$ and $[UO_2(I)_3]^-$, the position of ν_3 was determined by measuring the yield of the $[UO_2(X)_2]^-$ photodissociation product (reaction **2**) as a function of photon energy. This approach was necessary because the halide product generated by reaction **1** lies below the low-mass cutoff of the quadrupole instrument for each of the three precursors. It is not clear why reaction **2** was not observed in the earlier experiments performed using the FT-ICR instrument.

In the present study, no photodissociation product ions were observed for the $[UO_2(F)_3]^-$ precursor. For this species, the position

of ν_3 was instead measured by monitoring the depletion in precursor ion intensity as a function of photon energy. Previous DFT calculations suggest that the reaction energy to produce $[UO_2(F)_2]^-$ by loss of neutral fluorine radical would be ~37–70 kcal/mol higher than for the other precursor ions [34], making dissociation by reaction **2** unlikely. The F^- product ion (*m/z* 19) that might be generated by reaction **1** also lies below the low-mass cutoff of the quadrupole ion trap. To ensure that there is no loss in accuracy by measuring ν_3 by precursor ion depletion, the IRMPD of $[UO_2(Cl)_3]^-$ was examined using both modes. As shown in Fig. 1, the spectrum produced by monitoring depletion of $[UO_2(Cl)_3]^-$ as a function of photon energy (top trace) mirrors the spectrum generated by monitoring the photodissociation product ion yield (bottom trace, using formation of the $[UO_2(Cl)_2]^-$ by reaction **2**).

The IRMPD spectra for all four $[UO_2(X)_3]^-$ complexes are compared in Fig. 2. No peaks corresponding to the symmetric O=U=O stretch were observed in the IRMPD spectra, regardless of the species. All U-X stretch frequencies (expected to be in the range of 200 cm^{-1} to 600 cm^{-1}) lie below the lower frequency limit of the free electron laser under the operating conditions used in these experiments, and were not measured. The measured asymmetric stretching frequencies (ν_3) values for $[UO_2(I)_3]^-$, $[UO_2(Br)_3]^-$ and $[UO_2(Cl)_3]^-$ were 948 cm^{-1}, 942 cm^{-1} and 936 cm^{-1}, respectively. These results are in excellent agreement with the measured values from our previous study and demonstrates the reproducibility of the IRMPD experiments when using different ion trapping instruments. More importantly, the ν_3 value measured for $[UO_2(F)_3]^-$ was 893 cm^{-1}, which is 43 cm^{-1} lower than the one measured for $[UO_2(Cl)_3]^-$.

3.2. Computed asymmetric O=U=O stretching frequencies

As in the initial study of these species, the single minimum identified here for $[UO_2(X)_3]^-$ has trigonal bipyramidal geometry with axial oxo ligands, and the halide ligands occupying equatorial sites (Fig. 3). As noted earlier, we used multiple functionals and basis sets to ensure that a consistent trend with respect to the shift

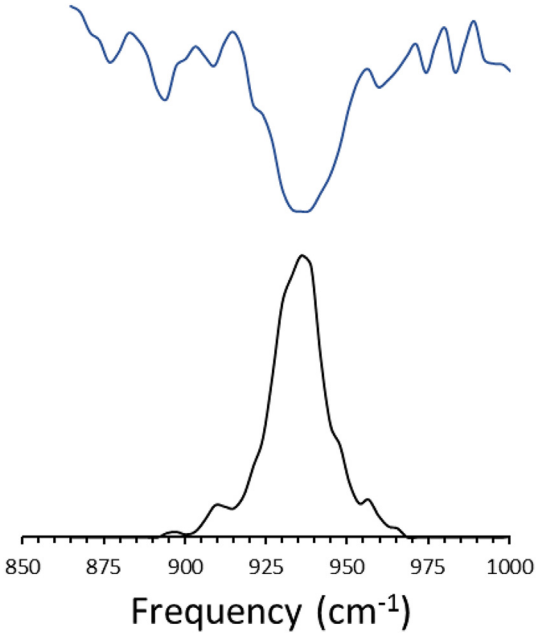

Fig. 1. Comparison of the vibrational action spectra for $[U^{VI}O_2(Cl)_3]^-$ recorded using depletion of precursor ion (top trace) and by photodissociation involving elimination of Cl radical to generate $[U^{V}O_2(Cl)_2]^-$.

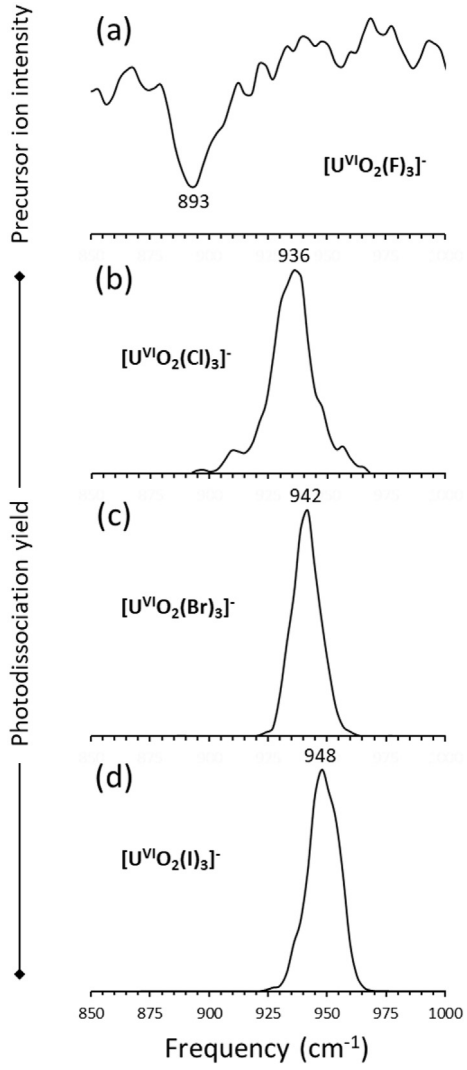

Fig. 2. Comparison of vibrational action spectra for (a) $[U^{VI}O_2(F)_3]^-$, (b) $[U^{VI}O_2(Cl)_3]^-$, (c) $[U^{VI}O_2(Br)_3]^-$ and (d) $[U^{VI}O_2(I)_3]^-$ using irradiation in a quadrupole ion trap instrument.

in ν_3 frequency with change in halide ligand was predicted by DFT. The unscaled computed ν_3 frequencies generated in the present study using the B3LYP functional, MWB46 and MWB60 pseudopotential on I and U, respectively, and either the 6-311 + G(d), 6-311 + G(3df) or aug-cc-pvtz basis set on O, F, Cl and Br are compared in Table 1. The computed ν_3 frequencies generated using the B3LYP, M06-L, PBE0 and SVWN functional, and the MWB46 and MWB60 pseudopotential on I and U, respectively, and the 6-311 + G(d) set on O, F, Cl and Br are compared in Table 2. As in the earlier study, the difference between the computed frequency for $[UO_2(Cl)_3]^-$, $[UO_2(Br)_3]^-$ and $[UO_2(I)_3]^-$ is ~7–10 cm^{-1}. Importantly, the computed ν_3 frequency for $[UO_2(F)_3]^-$ is 45 cm^{-1}, 49 cm^{-1} and 51 cm^{-1} lower than the frequency predicted for $[UO_2(Cl)_3]^-$ when using the 6-311 + G(d), 6-311 + G(3df) and aug-cc-pvtz basis set, respectively, on O, F, Cl and Br. A difference of 48 cm^{-1} was predicted in the earlier study.

The unscaled computed ν_3 frequencies computed using the B3LYP functional, MWB60 and MWB46 effective core potential/basis set on U and I, respectively, and either the 6-311 + G(d), 6–311+(3df) or aug-cc-pvtz basis set on O, F, Cl and Br, are compared to the experimental values in Fig. 4. In Fig. 5, the measured values are compared to the computed ν_3 frequencies

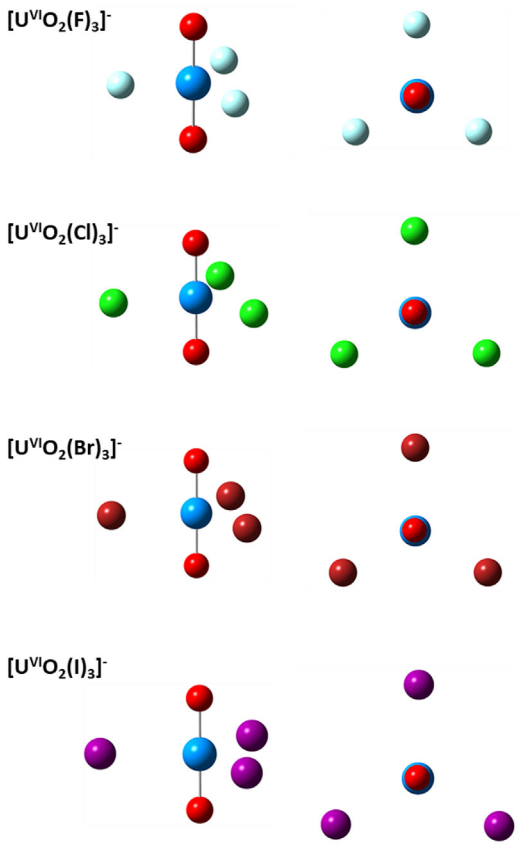

Fig. 3. Computed structures for $[U^{VI}O_2(X)_3]^-$, X = F, Cl, Br or I. Structures optimized using the B3LYP functional, MWB46 and MWB60 pseudopotential on I and U, respectively, and 6-311 + G(d) basis set on O, F, Cl and Br. Color code: U - blue; O - light red; F - sky blue; Cl - green; Br - dark red; I - purple. (For interpretation of the references to colour in this figure legend, the reader is referred to the Web version of this article.)

Table 1
Unscaled, computed asymmetric O=U=O stretching frequencies for $[U^{VI}O_2(X)_3]^-$, X = F, Cl, Br or I, using B3LYP functional and either the 6-311 + G(d), 6-311 + G(3df) or aug-cc-pvtz basis set on O, F, Cl and Br. *The MWB46 and MWB60 pseudopotentials with associated basis sets were used on I and U, respectively.

Halide	Basis set*			IRMPD
	6-311 + G(d)	6-311+(3df)	aug-cc-pvtz	
F	917	914	919	893
Cl	962	963	970	936
Br	968	970	977	942
I	978	981	988	948

Table 2
Unscaled, computed asymmetric O=U=O stretching frequencies for $[U^{VI}O_2(X)_3]^-$, X = F, Cl, Br or I, using the MWB46 and MWB60 pseudopotential on I and U, respectively, 6-311 + G(d) basis set on O, F, Cl and Br and either the B3LYP, M06-L, PBE0 or SVWN functional.

Halide	Functional				IRMPD
	B3LYP	M06-L	PBE0	LDA	
F	917	905	955	901	893
Cl	962	957	1000	942	936
Br	968	962	1007	947	942
I	978	971	1018	956	948

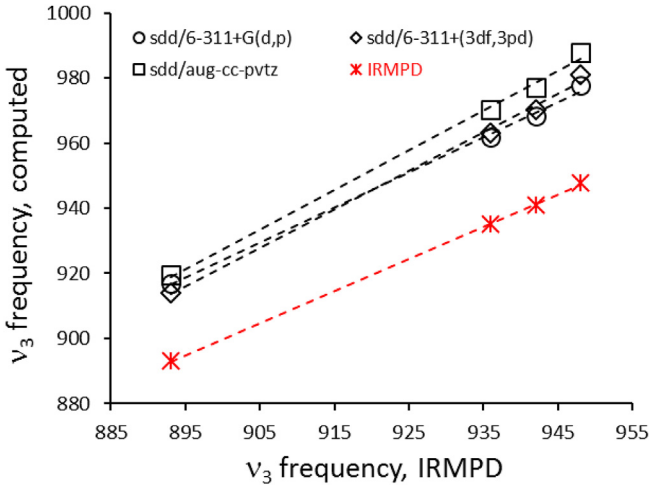

Fig. 4. Comparison of the experimental asymmetric O=U=O stretching frequency, ν_3, to computed values. Comparison made using the B3LYP functional, MWB46 and MWB60 pseudopotential on I and U, respectively, and either the 6-311 + G(d), 6-311 + G(3df) or aug-cc-pvtz basis set on O, F, Cl and Br.

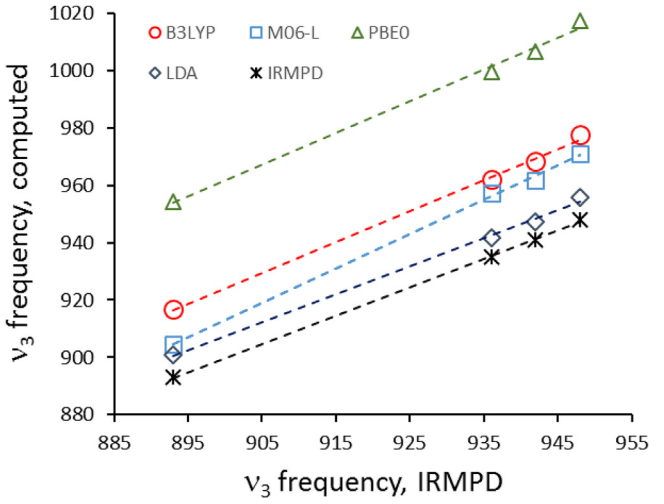

Fig. 5. Comparison of the experimental asymmetric O=U=O stretching frequency, ν_3, to computed values. Comparison made using the MWB46 and MWB60 pseudopotential on I and U, respectively, 6-311 + G(d) basis set on O, F, Cl and Br and either the B3LYP, M06-L, PBE0 or SVWN functional.

generated using the B3LYP, M06-L, PBE0 or SVWN functional, the MWB60 and MWB46 effective core potential/basis set on U and I, respectively, and either the 6-311 + G(d) basis set on the O, F, Cl and Br atoms. The comparison shows that the computed frequencies for ν_3 are sensitive to the choice in functional, however, each functional/basis set combination accurately captures the trend with respect to the dependence of ν_3 on the halide ligand X. In general, the local spin density approximation (SVWN functional) provides computed frequencies that lie closest to the measured values, while the PBE0 functional appears to be least accurate for predicting ν_3. The better agreement when using the SVWN functional is in accord with earlier investigations of U species [12,13,45–47]. When used for comparison to IRMPD measurements, unscaled computed ν_3 frequencies using the local density approximation were between 10 and 15 cm^{-1} higher for $[UO_2(aco)_n]^{2+}$ (n = 2–4) and 5 to 10 cm^{-1} higher for $[UO_2(acn)_n]^{2+}$ (n = 3–5) ions, whereas the discrepancy was greater by nearly a factor of 2 when using B3LYP [12]. Similar results were observed in an IRMPD study of the uranyl-nitrate

anion $[UO_2(NO_3)_3]^-$ [13].

As noted above, the ν_3 stretching frequency is sensitive to the degree to which electron density is donated to UO_2^{2+} by coordinating nucleophiles [29-37,48-51], with significant evidence for this coming from species-specific measurements in the gas phase [12-14,34,27,28]. The ν_3 value for $[UO_2(F)_3]^-$ of 893 cm^{-1}, reported here, can be compared to those for a series of cationic and anionic complexes with ligands of varying basicity. In the first systematic species-specific investigation using IRMPD, the lowest frequencies measured were 988 cm^{-1} and 1019 cm^{-1} for $[UO_2(aco)_4]^{2+}$ and 995 for $[UO_2(acn)_5]^{2+}$, respectively [13]. In a later study with a larger set of ligands, the ν_3 value for cations with general formula $[UO_2(L)_3]^{2+}$, where L = acetone, dimethylformamide (DMF), dimethyl sulfoxide (DMSO), tetramethyl urea (TMU) and tetramethylthiourea (TMTU) were 1000 cm^{-1}, 979 cm^{-1}, 973 cm^{-1}, 965 cm^{-1} and 954 cm^{-1}, respectively [28]. The values measured with TMU and TMTU as the coordinating ligands were lower than the ν_3 frequency for $U^{VI}O_2^{2+}$ coordinated by 2 oxo-glutaramide ligands (measured at 965 cm^{-1} [27]). The values observed when using the urea, thiourea and glutaramide ligands approached those measured for the reduced complexes $[UO_2(H_2O)]^+$ and $[UO_2(CH_3OH)]^+$, (952 cm^{-1} and 945 cm^{-1}, respectively) [13], which demonstrated the high degree of donation from ligand to the metal center. For anionic species, a ν_3 value of 949 cm^{-1} was measured for $[UO_2(NO_3)_3]^-$ [14]; and at 929 cm^{-1} and 938 cm^{-1} for the acetate and benzoate complexes $[UO_2(O_2C{-}CH_3)_3]^-$ and $[UO_2(O_2C{-}C_6H_5)_3]^-$, respectively [53]. Therefore, to the best of our knowledge, the ν_3 value for $[UO_2(F)_3]^-$, at 893 cm^{-1}, is the lowest yet reported for ν_3 in an IRMPD measurement.

4. Conclusions

To summarize, these experiments demonstrate that earlier predictions about the influence of halide ligands on the position of the ν_3 vibration in suite of complexes $[UO_2(X)_3]^-$ hold, with a modest red shift following the trend I < Br < Cl and significantly greater red shift for X = F. Based on our new experiments, we now show that the value measured for $[UO_2(F)_3]^-$ is ~43 cm^{-1} lower than the one measured for $[UO_2(Cl)_3]^-$, which is consistent with predictions made using DFT calculations.

The trends predicted by DFT, regardless of the limited group of functionals and basis sets employed here, are in excellent agreement with the measured shift in ν_3 frequency. With addition in the present study of F^- as a coordinating ligand, the trend with respect to the measured values of ν_3 in $[UO_2(X)_3]^-$ is consistent with the relative strengths of the halides as donor ligands. For example, based on a joint computational and gas-phase photoelectron spectroscopy study, Wang, Li, and coworkers [48] reported that U-X bonding within $[UO_2(X)_3]^-$ species, which is primarily ionic in character, is strongest for X = F, and progressively weaker for X = Cl, Br and I. In particular, they suggested that U–O orbitals are destabilized and become the frontier molecular orbitals in the fluoride complex through mixing with the low-energy F 2p orbitals. The U–O orbitals are instead stabilized and lie below the halogen lone-pair orbitals for the chloro-, bromo- and iodo-complexes. In total, the trend in ν_3 frequency is also consistent with the relative positions of the halides in the spectrochemical series, and the relative strengths of the respective nucleophiles polar, aprotic solvents.

Acknowledgements

MVS and TAC acknowledge support for this work in the form of start-up funds from the Bayer School of Natural and Environmental Sciences (BSNES) and Duquesne University. Laboratory space renovation at Duquesne University was made possible through support by the National Science Foundation (NSF) through grant CHE-0963450. Quantum mechanical calculations were performed using the resources of the Duquesne University Center for Computational Studies, and support from the National Science Foundation (CHE-1726824). A.B. acknowledges BSNES, Duquesne University and the National Science Foundation (CHE-1659823) for support of summer undergraduate research. C.G. and L.M. acknowledge BSNES and the Duquesne University Forensic Science and Law program for travel support. This work was also supported in part by the Robert Dean Loughney Faculty Development Endowment of Duquesne University. JM, GB and JO acknowledge support from the Netherlands Organisation for Scientific Research (NWO) under vici-grant no. 724.011.002 and the Stichting Physica. The authors also thank Britta Redlich and the FELIX facility staff for their invaluable assistance with portions of this work.

Appendix A. Supplementary data

Supplementary data to this article can be found online at https://doi.org/10.1016/j.ijms.2019.116231.

References

[1] F. Weigel, in: J.J. Katz, L.R. Morss, G.T. Seaborg (Eds.), The Chemistry of the Actinide Elements, Chapman and Hall, London, 1986, p. 169.
[2] N.N. Greenwood, A. Earnshaw, Chemistry of the Elements, Butterworth Heinemann, Oxford, Great Britain, 1997.
[3] W.M. Murphy, E.L. Shock, in: P.C. Burns, R. Finch (Eds.), Uranium: Mineralogy, Geochemistry and the Environment, Mineralogical Society of America, Washington, D. C., 1999, p. 221.
[4] D.G. Brookins, Geochemical Aspects of Radioactive Waste Disposal, Springer-Verlag, New York, 1984.
[5] G.R. Agnes, G. Horlick, Electrospray mass spectrometry as a technique for elemental analysis: preliminary results, Appl. Spectrosc. 46 (1992) 401–406.
[6] M.J. Van Stipdonk, W. Chien, V. Anbalagan, K. Bulleigh, D. Hanna, G. Groenewold, Gas-phase complexes containing the uranyl ion and acetone, J. Phys. Chem. A 108 (2004) 10448–10457.
[7] M.J. Van Stipdonk, W. Chien, K. Bulleigh, Q. Wu, G.S. Groenewold, Gas-phase uranyl-nitrile complex ions, J. Phys. Chem. A 110 (2006) 959–970.
[8] M. Van Stipdonk, G. Gresham, G. Groenewold, V. Anbalagan, D. Hanna, W. Chien, Elucidation of the collision-induced dissociation pathways of water and alcohol coordinated complexes containing the uranyl cation, J. Am. Soc. Mass Spectrom. 14 (2003) 1205–1214.
[9] W. Chien, D. Hanna, V. Anbalagan, G. Gresham, G. Groenewold, M. Zandler, M. Van Stipdonk, Intrinsic hydration of uranyl-hydroxide, -nitrate and -acetate complexes, J. Am. Soc. Mass Spectrom. 15 (2004) 777–783.
[10] G.S. Groenewold, M.J. Van Stipdonk, G.L. Gresham, W. Chien, K. Bulleigh, A. Howard, CID MS/MS of desferrioxamine siderophore complexes from ESI of UO_2^{2+}, Fe^{3+} and Ca^{2+} solutions, J. Mass Spectrom. 39 (2004) 752–761.
[11] M. Van Stipdonk, W. Chien, V. Anbalagan, G.L. Gresham, G.S. Groenewold, Oxidation of 2-propanol ligands during collision-induced dissociation of a gas-phase uranyl complex, Int. J. Mass Spectrom. 237 (2004) 175–183.
[12] G.S. Groenewold, A.K. Gianotto, K.C. Cossel, M.J. Van Stipdonk, D.T. Moore, N. Polfer, J. Oomens, W.A. de Jong, L. Visscher, Vibrational spectroscopy of mass-selected $[UO_2(ligand)_n]^{2+}$ complexes in the gas phase: comparison with theory, J. Am. Chem. Soc. 128 (2006) 4802–4813.
[13] G.S. Groenewold, J. Oomens, W.A. de Jong, G.L. Gresham, M.E. McIlwain, M.J. Van Stipdonk, Vibrational spectroscopy of anionic nitrate complexes of UO_2^{2+} and Eu^{3+} isolated in the gas phase, Phys. Chem. Chem. Phys. 10 (2008) 1192–1202.
[14] G.S. Groenewold, M.J. Van Stipdonk, W.A. de Jong, J. Oomens, G.L. Gresham, M. McIlwain, D. Gao, B. Siboulet, L. Visscher, M. Kullman, N. Polfer, Infrared spectroscopy of dioxouranium(V) complexes with solvent molecules: effect of reduction, ChemPhysChem 9 (2008) 1278–1285.
[15] G.S. Groenewold, M.J. van Stipdonk, J. Oomens, W.A. de Jong, M.E. McIlwain, The gas-phase bis-uranyl nitrate complex $[(UO_2)_2(NO_3)_5]^-$: infrared spectrum and structure, Int. J. Mass Spectrom. 308 (2011) 175–180.
[16] M.J. Van Stipdonk, M.C. Michelini, A. Plaviak, D. Martin, J.K. Gibson, Formation of bare UO_2^{2+} and NUO^+ by fragmentation of gas-phase uranyl-acetonitrile complexes, J. Phys. Chem. A 118 (2014) 7838–7846.
[17] M.J. Van Stipdonk, C. O'Malley, A. Plaviak, D. Martin, J. Pestok, P.A. Mihm, C.G. Hanley, T. Corcovilos, J.K. Gibson, B.J. Bythell, Dissociation of gas-phase, doubly-charged uranyl-acetone complexes by collisional activation and infrared photodissociation, Int. J. Mass Spectrom. 396 (2016) 22–34.
[18] P.D. Dau, D. Rios, Y. Gong, M.C. Michelini, J. Marçalo, D.K. Shuh, M. Mogamman, M.J. Van Stipdonk, T.A. Corcovilos, J. Martens, J. Oomens, B. Redlich, J.K. Gibson, Synthesis and hydrolysis of uranyl, neptunyl and plutonyl gas-phase complexes exhibiting discrete actinide-carbon bonds,

Organometallics 35 (2016) 1228–1240.
[19] M.J. Van Stipdonk, C. Hanley, E. Perez, J. Pestok, P. Mihm, T.A. Corcovilos, Collision-induced dissociation of uranyl-methoxide and uranyl-ethoxide cations: formation of UO_2H^+ and uranyl-alkyl product ions, Rapid Commun. Mass Spectrom. 30 (2016) 1879–1890.
[20] E. Perez, C. Hanley, S. Koehler, J. Pestok, N. Polonsky, M.J. Van Stipdonk, Gas phase reactions of ions derived from anionic uranyl formate and uranyl acetate complexes, J. Am. Soc. Mass Spectrom. 27 (2016) 1989–1998.
[21] S.X. Hu, J.K. Gibson, W.L. Li, M.J. Van Stipdonk, J. Martens, G. Berden, B. Redlich, J. Oomens, J. Li, Electronic structure and characterization of a uranyl di-15-crown-5 complex with unprecedented sandwich structure, Chem. Commun. (J. Chem. Soc. Sect. D) 52 (2016) 12761–12764.
[22] M.J. Van Stipdonk, I. Tatosian, A. Bubas, E. Perez, N. Polonsky, L. Metzler, A. Somogyi, Formation of $[U^{V}OF_4]^-$ by collision-induced dissociation of a $[U^{VI}O_2(O_2)(O_2C\text{-}CF_3)_2]^-$ precursor, Int. J. Mass Spectrom. 424 (2018) 58–64.
[23] J. Jian, S.X. Hu, W.L. Li, M.J. van Stipdonk, J. Martens, G. Berden, J. Oomens, J. Li, J.K. Gibson, Uranyl-(12-Crown-4) ether complexes and derivatives: structural characterization and isomeric differentiation, Inorg. Chem. 57 (2018) 4125–4134.
[24] I.J. Tatosian, A.C. Iacovino, M.J. Van Stipdonk, CID of $[UO_2ClO_4]^+$ revisited: production of $[UO_2Cl]^+$ and subsequent hydrolysis to create $[UO_2OH]^+$, Rapid Commun. Mass Spectrom. 32 (2018) 1085–1091, 2018.
[25] M.J. Van Stipdonk, A. Iacovino, I. Tatosian, Influence of background H_2O on the collision-induced dissociation products generated from $[UO_2NO_3]^+$, J. Am. Soc. Mass Spectrom. 29 (2018) 1416–1424.
[26] M.J. van Stipdonk, I.J. Tatosian, A.C. Iacovino, A.R. Bubas, L. Metzler, M.C. Sherman, A. Somogyi, Gas-phase deconstruction of UO_2^{2+}: mass spectrometry evidence for generation of $[OU^{VI}CH]^+$ by collision-induced dissociation of $[U^{VI}O_2(C{\equiv}CH)]^+$, J. Am. Soc. Mass Spectrom. 30 (2019) 796–805.
[27] J.K. Gibson, H.S. Hu, M.J. Van Stipdonk, G. Berden, J. Oomens, J. Li, Infrared multiphoton dissociation spectroscopy of a gas-phase complex of uranyl and 3-Oxa-glutaramide: an extreme red-shift of the $[O{=}U{=}O]^{2+}$ asymmetric stretch, J. Phys. Chem. A 119 (2015) 3366–3374.
[28] J.K. Gibson, W.A. de Jong, M.J. van Stipdonk, J. Martens, G. Berden, J. Oomens, Equatorial coordination of uranyl: correlating ligand charge donation with the U-O-yl asymmetric Stretch frequency, J. Organomet. Chem. 857 (2018) 94–100.
[29] S.P. Mcglynn, W.C. Neely, J.K. Smith, Electronic structure, spectra, and magnetic properties of oxycations. 3. Ligation effects on infrared spectrum of uranyl ion, J. Chem. Phys. 35 (1961) 105–116.
[30] L.J. Basile, J.C. Sullivan, J.R. Ferraro, P. Labonville, Raman-scattering of uranyl and transuranium V, VI, and VII ions, Appl. Spectrosc. 28 (1974) 142–145.
[31] C. Nguyen-Trung, G.M. Begun, D.A. Palmer, Aqueous uranium complexes. 2. Raman-spectroscopic study of the complex-formation of the dioxouranium(VI) ion with a variety of inorganic and organic-ligands, Inorg. Chem. 31 (1992) 5280–5287.
[32] M.J. Sarsfield, M. Helliwell, J. Raftery, Distorted equatorial coordination environments and weakening of U=O bonds in uranyl complexes containing NCN and NPN ligands, Inorg. Chem. 43 (2004) 3170–3179.
[33] P. Di Pietro, A. Kerridge, U-O-yl stretching vibrations as a quantitative measure of the equatorial bond covalency in uranyl complexes: a quantum chemical investigation, Inorg. Chem. 55 (2016) 573–583.
[34] S. Tsushima, On the "yl" bond weakening in uranyl(VI) coordination complexes, Dalton Trans. 40 (2011) 6732–6737.
[35] C. Nguyen-Trung, D.A. Palmer, G.M. Begun, C. Peiffert, R.E. Mesmer, J. Solut. Chem. 29 (2000) 101–129.
[36] F. Quilès, A. Burneau, Infrared and Raman spectra of uranyl(VI) oxo-hydroxo complexes in acid aqueous solutions: a chemometric study, Vib. Spectrosc. 23 (2000) 231–241.
[37] F. Quilès, A. Burneau, Infrared and Raman spectroscopic study of uranyl complexes: hydroxide and acetate derivatives in aqueous solution, Vib. Spectrosc. 18 (1998) 61–75.
[38] G.S. Groenewold, M.J. van Stipdonk, J. Oomens, W. de Jong, G.L. Gresham, M.E. McIlwain, Vibrational spectra of discrete UO_2^{2+} halide complexes in the gas phase, Int. J. Mass Spectrom. 297 (2010) 67–75.
[39] D. Oepts, A.F.G. van der Meer, P.W. van Amersfoort, The Free-electron-laser user facility FELIX, Infrared Phys. Technol. 36 (1995) 297–308.
[40] L.J.M. Kempkes, J.K.M. Martens, J. Grzetic, G. Berden, J. Oomens, Deamidation reactions of protonated asparagine and glutamine investigated by ion spectroscopy, Rapid Commun. Mass Spectrom. 30 (2016) 483–490.
[41] A.D. Becke, Density-functional thermochemistry. III. The role of exact exchange, J. Chem. Phys. 98 (1993) 5648–5652.
[42] C. Lee, W. Yang, R.G. Parr, Development of the Colle-Salvetti correlation-energy formula into a functional of the electron density, Phys. Rev. B 37 (1988) 785–789.
[43] P.J. Stephens, F.J. Devlin, C.F. Chabalowski, M.J. Frisch, Ab Initio calculation of vibrational absorption and circular dichroism spectra using density functional force fields, J. Phys. Chem. 98 (1994) 11623–11627.
[44] J.P. Perdew, M. Ernzerhof, K. Burke, Rationale for mixing exact exchange with density functional approximations, J. Chem. Phys. 105 (1996) 9982–9985.
[45] C. Adamo, V. Barone, Toward reliable density functional methods without adjustable parameters: the PBE0 model, J. Chem. Phys. 110 (1999) 6158–6170.
[46] Y. Zhao, D.G. Truhlar, The M06 suite of density functionals for main group thermochemistry, thermochemical kinetics, noncovalent interactions, excited states, and transition elements: two new functionals and systematic testing of four M06-class functionals and 12 other functionals, Theor. Chem. Acc 120 (2008) 215–241.
[47] S.H. Vosko, L. Wilk, M. Nusair, Accurate spin-dependent electron liquid correlation energies for local spin density calculations: a critical analysis, Can. J. Phys. 58 (1980) 1200–1211.
[48] V. Vallet, U. Wahlgen, I. Grenthe, Probing the nature of chemical bonding in uranyl(VI) complexes with quantum chemical methods, J. Phys. Chem. A 116 (2012) 12373–12380.
[49] J. Su, P.D. Dau, Y.-H. Qui, H.-T. Liu, C.-F. Xu, D.-L. Huang, L.-S. Wang, J. Li, Probing the electronic structure and chemical bonding in tricoordinate uranyl complexes UO_2X_3 (X=F, Cl, Br, I): competition between coulomb repulsion and U-X bonding, Inorg. Chem. 52 (2013) 6617–6626.
[50] W.A. De Jong, E. Aprà, T.L. Windus, J.A. Nichols, R.J. Harrison, K.E. Gutowski, D.A. Dixon, J. Phys. Chem. A 109 (2015) 11568–11577.
[51] V.E. Jackson, R. Craciun, D.A. Dixon, K.A. Peterson, W.A. de Jong, J. Phys. Chem. A 112 (2008) 4095–4099.
[52] M.J. Frisch, G.W. Trucks, H.B. Schlegel, G.E. Scuseria, M.A. Robb, J.R. Cheeseman, G. Scalmani, V. Barone, G.A. Petersson, H. Nakatsuji, X. Li, M. Caricato, A. Marenich, J. Bloino, B.G. Janesko, R. Gomperts, B. Mennucci, H.P. Hratchian, J.V. Ortiz, A.F. Izmaylov, J.L. Sonnenberg, D. Williams-Young, F. Ding, F. Lipparini, F. Egidi, J. Goings, B. Peng, A. Petrone, T. Henderson, D. Ranasinghe, V.G. Zakrzewski, J. Gao, N. Rega, G. Zheng, W. Liang, M. Hada, M. Ehara, K. Toyota, R. Fukuda, J. Hasegawa, M. Ishida, T. Nakajima, Y. Honda, O. Kitao, H. Nakai, T. Vreven, K. Throssell, J.A. Montgomery Jr., J.E. Peralta, F. Ogliaro, M. Bearpark, J.J. Heyd, E. Brothers, K.N. Kudin, V.N. Staroverov, T. Keith, R. Kobayashi, J. Normand, K. Raghavachari, A. Rendell, J.C. Burant, S.S. Iyengar, J. Tomasi, M. Cossi, J.M. Millam, M. Klene, C. Adamo, R. Cammi, J.W. Ochterski, R.L. Martin, K. Morokuma, O. Farkas, J.B. Foresman, D.J. Fox, Gaussian 09, Revision A.02, Gaussian, Inc., Wallingford CT, 2016.
[53] G.S. Groenewold, W.A. de Jong, J. Oomens, M.J. Van Stipdonk, Variable denticity in carboxylate binding to the uranyl coordination complexes, J. Am. Soc. Mass Spectrom. 21 (2010) 719–727.